

**BATSE SOFT GAMMA-RAY OBSERVATIONS OF
GROJ0422+32**

J. C. Ling

Jet Propulsion Laboratory 169-327, California Institute of Technology

4800 Oak Grove Drive, Pasadena, CA 91109

`james.c.ling@jpl.nasa.gov`

and

Wm. A. Wheaton

Infrared Processing and Analysis Center, California Institute of Technology

100-22, Pasadena, CA 91125

`waw@ipac.caltech.edu`

Received 3 Sep 2002; accepted 15 Oct 2002

To appear in the February 10, 2003 issue of *Astrophysical Journal*

ABSTRACT

We report results of a comprehensive study of the soft gamma-ray (30 keV to 1.7 MeV) emission of GROJ0422+32 during its first known outburst in 1992. These results were derived from the BATSE earth-occultation database with the JPL data analysis package, EBOP (Enhanced BATSE Occultation Package). Results presented here focus primarily on the long-term temporal and spectral variability of the source emission associated with the outburst, which complement those reported earlier by BATSE (Harmon et al. 1993, Ling et al. 2000), OSSE (Grove et al. 1998), COMPTEL (Van Dijk et al. 1995) and SIGMA (Sunyaev et al. 1993; Roques et al. 1994).

The light curves with 1-day resolution in six broad energy-bands (e.g. 35-100 keV, 100-200 keV, 200-300 keV, 300-400 keV, 400-700 keV and 700-1000 keV) show the high-energy flux (>200 keV) led the low-energy flux (<200 keV) by ~ 5 days in reaching the primary peak, but lagged the latter by ~ 7 days in starting the declining phase. We confirm the "secondary maximum" of the low-energy (<200 keV) flux at \sim TJD 8970-8981, ~ 120 days after the first maximum, reported earlier by the BATSE team (Harmon et al. 1993). Our data show that the "secondary maximum" was also prominent in the 200-300 keV band, but became less pronounced at higher energies.

During this 200-day period, the spectrum evolved from a power-law with photon index of 1.75 on TJD 8839, to a shape that can be described by a Comptonized model or an exponential power law below 300 keV, with a variable power-law tail above 300 keV. The spectrum remained roughly in this two-component shape until ~ 9 November (TJD 8935) when the 35-429 keV luminosity dropped to below $\sim 20\%$ of its peak value observed on TJD-8848. It then returned to the initial power-law shape with an index of ~ 2 and stayed in this shape until the end

of the period. The correlation of the two spectral shapes (e.g. Compton/power law tail vs. power law) with the high and low luminosities of the soft gamma-ray emission is strongly reminiscent of that seen in Cygnus X-1, suggesting that similar processes are at work in both systems. We observed also four separate episodes of high-energy (400-1000 keV) emission during the first 84 days of the event. We interpret these results in terms of the Advection Dominated Accretion Flow (ADAF) model with possibly a "jet-like" region that persistently produced the non-thermal power-law gamma rays observed throughout the event.

Subject headings: gamma-rays observations—Black Holes —individual (GROJ0422+32)

1. INTRODUCTION

The γ -ray source GROJ0422+32 was first discovered by The Burst and Transient Source Experiments (BATSE; Fishman et al. 1989) onboard the Compton Observatory on August 5th 1992 (Paciesas et al. 1992). Early BATSE results (Harmon et al 1992, 1994) reported by the MSFC PI team showed that the source underwent a major outburst when the hard x-ray (40-230 keV) flux reached a level of ~ 3 Crab in about three days. It remained at this level for approximately three days and then decreased exponentially with a time constant of 43.6 days (Vikhlinin et al. 1995). A secondary maximum was then observed approximately 120 days after the first maximum, in December 1992 (Harmon et al. 1994), again followed by an exponential decay with time scale similar to that of the first maximum. The entire outburst lasted for about 200 days before returning to the pre-burst quiescent level.

Observational data in UV/Optical/IR/Radio (Castro-Tirado et al. 1992, 1993; Wagner

et al. 1992; van Paradijs et al. 1994; Shrader et al. 1992a, b, 1994; Chevalier and Ilovaisky 1995, 1996; Bonnet-bidaud and Mouchet 1995; Callanan et al. 1996; Casares et al. 1995; Garcia et al. 1996) and in X-ray and γ -ray (Sunyaev et al. 1993; Pietsch et al. 1993; Harmon et al. 1994; Roques et al. 1994; Vikhlinin et al. 1995; and van Dijk et al. 1995; Grove et al. 1998; Ling et al. 2000; Iyudin & Haberl 2001) of this event and subsequent outbursts have also been reported in the literature. An optical counterpart of GROJ0422+32 was observed by Castro-Tirado et al (1992, 1993) and Wagner et al. (1992) showing a visual magnitude of $V = 13$ at the peak of the event. The optical lightcurve then declined exponentially with a time scale of 170 days (Shrader et al. 1994) and reached a quiescence level of $V = 22.35 \sim 800$ days after the discovery of the x-ray source (Garcia et al. 1996). The 9 magnitude change in V was the largest seen in any Soft X-ray Transients (SXT) to date (van Paradijs & McClintock 1995).

There was also evidence showing the source is a binary system. Filippenko, Matheson, & Ho (1995) observed a 5.08 ± 0.01 hour orbital period, and estimated a mass function of $f(M) = 1.21 \pm 0.06 M_{\odot}$ (where M_{\odot} is the solar mass). The mass function is consistent with $f(M) = 0.40 \pm 1.40 M_{\odot}$ reported by Orosz & Bailyn (1995), and $0.85 \pm 0.30 M_{\odot}$ reported by Casares et al. (1995). Using the orbital inclination of $i \leq 45^{\circ}$ determined by Callanan et al. (1996), the mass of the compact object is estimated to be $\geq 3.4 M_{\odot}$. However, based on the orbital inclination of $10^{\circ} - 31^{\circ}$ estimated independently from infrared and optical photometry, a lower limit of $\geq 9 M_{\odot}$ for the compact object is implied, which strongly suggested the existence of a black hole (BH) in the system. The distance of the source was estimated by Shrader et al (1994) to be 2.4 ± 0.4 kpc.

The BH nature of GROJ0422+32 was also supported by X and γ -ray observations. First, the contemporaneous x-ray and soft γ -ray spectra measured by TTM and HXTE instruments (Sunyaev et al. 1993; Maisack et al. 1994) in the 2 to 300 keV range, and

SIGMA (Roques et al. 1994) in the 35-600 keV range, onboard the Mir-Kvant spacecraft, and by BATSE (Harmon et al. 1994; Ling et al. 2000), OSSE (Grove et al. 1998) and COMPTEL (van Dijk et al. 1995) on the Compton Observatory in the 50 keV - 2 MeV range can generally be characterized by either an exponentially truncated power-law with a photon power-law index of 1.49 ± 0.01 , break energy E_b of 60 ± 3 keV, and e-folding energy E_f of 132 ± 2 keV, or in terms of a Comptonized disk model (Sunyaev & Titarchuk 1980) with a temperature of $kT \sim 58$ keV and an optical depth of ~ 2 . It is interesting to note that the SIGMA spectrum (Roques et al. 1994) shows excess flux from 400 to 600 keV above the best-fit Comptonized model, and that high-energy flux was also observed from 1-2 MeV by COMPTEL (van Dijk et al. 1995). The composite spectral shape, Comptonized below and power-law above 400 keV respectively (see Ling et al. 2000; Figure 3 panels 36-39) strongly resembles the standard-state (γ_2 , or x-ray low/hard-state) spectrum of Cygnus X-1 (Ling et al. 1987, 1997; McConnell et al. 2001), the best-known black-hole candidate in our galaxy.

Second, the timing analysis of the hard x-ray data of BATSE (20 - 300 keV; Kouveliotou et al. 1992, 1993; van der Hooft et al., 1999), and SIGMA (45 - 150 keV; Vikhlinin et al. 1995) showed evidence for low frequency quasi-periodic oscillation (QPOs) centered at 0.03 and 0.2 Hz for the former and 0.3 Hz for the latter. These results are consistent with the frequencies observed by OSSE (Grove et al. 1994). Because of similar low frequency QPO's observed in other black holes (BH; Sunyaev et al. 1991; Van der Klis 1994; Kouveliotou 1994), it is suggested (Roques et al. 1994) that the GROJ0422+32 could be a BH also.

While previous soft γ -ray results (30 keV to 2 MeV; Harmon et al. 1992, 1993, 1994; Sunyaev et al. 1993; Maisack et al. 1994; Roques et al. 1994; van Dijk et al. 1995; Grove et al. 1998; Ling et al. 2000) have advanced our understanding of the system, information concerning the long-term behavior of the source during the outburst, however, is far from

complete. The earlier BATSE published lightcurve (Paciesas et al. 1992; Harmon et al. 1992, 1993) primarily focused on the energy region below 200 keV. The spectra measured by COMPTEL, OSSE and SIGMA focused on only isolated periods of the 200-day event due in part to the relatively spotty coverage of pointed observations made by most of these experiments. Questions that need to be addressed include (1) how does the source spectrum evolve over the course of the event, and (2) what is the long-term behavior of the high-energy flux above 200 keV compared to that below 200 keV (Harmon et al. 1994; Grove et al. 1998)? Answers to these questions will shed further light on the mechanism driving the outburst, and ultimately the physical makeup of the system itself.

This paper addresses these important questions. Our results were obtained using BATSE Earth Occultation data provided by the BATSE PI team at MSFC (Fishman et al. 1989), processed and analyzed using the JPL Enhanced BATSE Occultation Package (EBOP; Ling et al. 1996, 2000). A brief description of the EBOP database and technique are given in Section 2. Results produced by EBOP are presented in Section 3.

2. EBOP Database and Technique

The BATSE Earth Occultation data were obtained by its eight Large Area NaI scintillator Detectors (LADs), each 50.8 cm diameter and 1.25 cm thick ($\sim 2025 \text{ cm}^2$ geometrical area) operating in the energy range 0.02 - 1.8 MeV (Fishman et al. 1989). These eight LADs were placed at the eight corners of the spacecraft and provided nearly isotropic response to $\sim 2/3$ of the sky that not occulted by the Earth. They were therefore ideally suited for unprecedented sensitive long-term continuous monitoring of gamma-ray sources, using the Earth occultation technique (Harmon et al. 1992, 2002; Ling et al. 2000). The BATSE Earth Occultation data provided by the MSFC PI team consisted of continuous (CONT) data in 16 energy-channels with 2.048-s resolution for each LAD. These

2.048-s resolution data were summed to 16.384-s resolution bins at JPL, and used as input to the EBOP analysis system (Ling et al. 1996, 2000). Due to uncertainties of the energy edges of the first and the last energy channels, we analyzed only the central 14 channels here. The 5274 16-s data bins in each day typically yielded ~ 4300 valid bins after losses and gaps. The heart of the EBOP system fitted these ~ 4300 measured count-rates (per day, per energy channel, and per LAD) to a linear model in ~ 45 - 75 unknown terms that typically included contributions from 10-40 point sources (of a total of 64 sources in the EBOP input catalog) and ~ 35 physical background terms. Since the source flux in each of the 14 energy bins, and for each LAD, was independently determined daily over a very distinct and highly variable background for the different LADs, a strength of the BATSE experiment and the EBOP system is the consistency check they provide on the source fluxes measured by the different LADs daily and over the 10-14 day viewing periods as shown in Section 3 (see also Wallyn et al. 2001).

3. Results

3.1. Flux Histories

Figure 1 shows the flux histories, with 1-day resolution, in the 35-100 keV, 100-200 keV, 200-300 keV, 300-400 keV, 400-700 keV, and 700-1000 keV energy bands, respectively, covering the period from 27 June 1992 (TJD 8800) to 23 April 1993 (TJD 9100). Highlights of these results include:

a. The 35-200 keV flux rose sharply after the onset of the outburst on 5 August 1992 (TJD 8839, labeled "1"), and reached the first of two maxima during the peak of the outburst on 14 August (TJD 8848, vertical dashed line "b"). It then decreased slightly ($\sim 5\%$ for 35-100 keV, and $\sim 6\%$ for 100-200 keV) over the next few days before rising again

to a second maximum on 21 August (TJD 8855, vertical dashed line "c"). The declining phase of the event took ~ 180 days. The combined 35-200 keV flux reached half the peak level on \sim TJD 8877, and a tenth of the peak on \sim TJD 8935, approximately 80 days later. It continued to decrease to a level about 4% of the peak value on TJD 8960 before slowly rising again to the so-called "secondary maximum" on TJD 8972 (~ 120 days after the primary maximum on \sim TJD 8852) at a level about 15% of the peak value. The 35-200 keV flux stayed within 20% of the "secondary maximum" for ~ 20 days before declining, and finally reached the "pre-outburst" quiescent level on TJD 9040.

b. We observed also for the first time energy-dependent flux variability above 200 keV (see Figure 1 panels 3-6). These data show temporal features significantly different than those observed below 200 keV. First, the high-energy flux rose more promptly after the onset and reached the 1st of four local maxima on TJD 8843 (vertical dashed line "a"), 5 days before the 1st maximum of the 35-200 keV flux (vertical dashed line "b"). It then declined in the next nine days before rising to a second maximum on 28 August (TJD 8862; vertical dashed line in panel "d"), 7 days after the second maximum (vertical dashed line in panel "c") and during the declining phase of the hard x-ray (35-200 keV) flux. The flux ratio of the 2nd maximum to 1st maximum increased with energies, ranging from ~ 1 for 200-300 keV, 1.3 for 300-400 keV, ~ 2 for 400-700 keV to ~ 3.3 for 700-1000 keV. The local minimum around TJD 8850 became more pronounced with increasing energy. The flux ratio of this minimum to the 2nd maximum decreased from ~ 0.9 for 200-300 keV, ~ 0.4 for 300-400 keV, ~ 0.2 for 400-700 keV to ~ 0 for 700-1000 keV. Variable high-energy fluxes were also consistently observed in the three high-energy channels (300-400 keV, 400-700 keV, and 700-1000 keV) in at least two other periods centered at \sim TJD 8889 (3rd maximum, vertical dashed line "e") and TJD 8919 (4th maximum, vertical dashed line "f"), interspersed with periods of low gamma-ray flux at \sim TJD 8875 and TJD 8900, respectively. Spectra measured during these highly variable gamma-ray flux periods are

presented in detail in the next section. The broad "secondary maximum" observed in 35-200 keV was also prominently observed in 200-300 keV at \sim TJD 8970-8981, \sim 120 days after the primary peak, but became less pronounced at higher energies. There is also a dip in intensity at around TJDs 8973-8977 in the midst of the "secondary maximum", similar to that seen in the primary peak. Such a dip is consistently seen in all six energy-bands. Its significance is estimated to be $\sim 5\sigma$ at 200-300 keV. Iyudin & Haberl (2001) showed that the gamma-ray emission, based on 25 observations by COMPTEL obtained between August 1992 and August 1997 (\sim 1800 days) and three Viewing Periods before the 1992 outburst, is primarily confined between 1.5 and 2 MeV, and was more prominent during phases from 0.0 to 0.5 of the 120d period, where zero phase corresponds to TJD 8840.5. Our BATSE results show that the high-energy fluxes were confined to phases from 0.0 to 0.7 of the same periodicity. The averaged flux of the 700-1000 keV emission integrated over TJD 8841-8923 (phase \sim 0-0.7) is $(1.6 \pm 0.3) \cdot 10^{-6}$ photons $\text{cm}^{-2}\text{-s}^{-1}\text{-keV}^{-1}$ compared to $(-4.9 \pm 5.1) \cdot 10^{-7}$ photons $\text{cm}^{-2}\text{-s}^{-1}\text{-keV}^{-1}$ integrated over TJD 8925-8960 (\sim phase 0.7-1.0). Similarly for the 400-700 keV emission, the averaged fluxes for the same two periods are $(10.0 \pm 0.6) \cdot 10^{-6}$ photons- $\text{cm}^{-2}\text{-s}^{-1}\text{-keV}^{-1}$ and $(1.3 \pm 0.8) \cdot 10^{-6}$ photons- $\text{cm}^{-2}\text{-s}^{-1}\text{-keV}^{-1}$, respectively.

3.2. Spectra

The complex energy-dependent flux histories shown in Figure 1 imply complex spectral changes over the course of the 200-day event. We selected a sample of thirty-six single-day spectra spanning the period from TJD 8839 to TJD 9033 to show such changes. Pertinent information related to each of these spectra is given in both Figure 2 and Table 1. For each day, the source was observed by two to four of the eight BATSE LADs with good sensitivity. These "source-viewing" LADs, which are identified in Table 1 and Figure 2, were selected using the criterion discussed by Ling et al. (1996, 2000). Each LAD spectrum has 14 energy

bins. The solid line is the best-fit model (either Compton model or power-law) to the n data points, where $n = \text{number of LADs} \times 14 \text{ energy channels}$, using the standard analysis fitting program XSPEC (Arnaud 1996). The best-fit model and parameters, as well as reduced χ^2 (χ^2/ν , where ν is the number of degrees of freedom) of the fit are also displayed in each panel and listed in Table 1. In twelve of the thirty-six panels (e.g. panels in the middle column in each of the four pages) in Figure 2, spectra measured simultaneously by all "source-viewing" LADs on that day are shown and compared. Since each LAD-spectrum was independently determined over a complex background that is totally different from that of the other seven LADs, these simultaneously measured spectra allow one to assess the quality and consistency of the results. Consistency of fluxes among all "source-viewing" LADs is also reflected by the goodness of the model fits to the data (Ling et al. 1996; Ling et al. 2000). Large reduced χ^2 could be caused by either inconsistency of LAD fluxes or inadequacy of the spectral model. Twenty-nine of the 36 spectra shown in Figure 1 have acceptable fits with either a power law or a Compton model. The relatively large reduced χ^2 shown in panels 13-21 (\sim TJD 8855-8883, taken around the 2nd maximum of the high-energy fluxes) are due primarily to a spectral tail above 300 keV. In general the consistency among LADs in the 36 spectra in Figure 2 gives us good confidence in the analysis technique and results. Having developed data analysis systems for four separate missions (e.g. OSO-7, HEAO-1, HEAO-3, and CGRO) in the past three decades, and shared the frustration of many others of the disparate results produced by different experiments, some of which could be caused by systematic effects associated with the inadequacy of the data analysis techniques, we believe it is useful to show internal consistency achieved among the relevant detectors of a single instrument, such as BATSE. This was an important goal for EBOP. We hope the results presented here will encourage other investigators to show internal consistency, as a necessary quality control requirement in future gamma-ray data analysis

Key spectral results shown in Figures 2 & 3 and Table 1 are summarized as follows:

3.2.1. High-State Spectrum and Variability

a. During the rising phase of the event, the single-day spectrum shown in Figure 2a changed from a power-law with photon index of 1.75 on TJD 8839 (Figure 2a panel 1) to two days later, a shape better characterized by a single temperature analytic Compton model (Sunyaev & Titarchuk 1980), with $kT = 59 \pm 5$ keV and $\tau = 2.27 \pm 0.19$, on TJD 8841 (Figure 2a-panel 2). The reduced χ^2 for a power-law fit to the TJD 8841 spectrum is 2.9 compared to 0.66 for the Compton model (see Table 1), clearly indicating the change in spectral shape. In fact, the 4-day averaged spectra measured by the two "source-viewing" LADs (1 & 5) during Viewing-Period 35 (VP-35 TJD 8841-8844; see Figure 3a - panel 1) show excesses of the high-energy (>300 keV) flux over the best-fit Compton model (solid line - $kT = 51.1$ keV, $\tau = 2.93$). The dashed line is the best-fit power law ($\alpha = 3.4$) to the flux in the five high-energy channels (313 - 1700 keV) measured by the two "source-viewing" LADs (1 & 5). Such high-energy flux was only hinted in the corresponding single-day spectra (Figure 2a panels 2-5) due to statistical limitation of the data. The two-component (Compton + power law) spectrum is strongly reminiscent of the γ_2 spectrum (or "low/hard" X-ray state) of Cygnus X-1 (Ling et al. 1997; McConnell et al. 2000; Ling 2001), suggesting similar physical processes were at work in both systems.

b. Figure 2-a,b,c panels 6-25 and Figure 3-a,b panels 2-8 show the single-day and multiple-day VP spectra, respectively, covering the period from TJD 8847 to 8925. This period includes: (1) the peak and decay phases of the event when the 35-429 keV luminosity was above 20% of the peak value (see Table 1), and (2) periods of the 2nd (vertical dashed line "e") and 3rd (vertical dashed line "f") high-energy peaks described in Section 3.1. During this 78-day period, the spectrum underwent significant changes. For the low-energy

Comptonized component below 300 keV, as reflected by the best-fit parameters of the single-day spectrum shown in Table 1, the electron temperature (kT) varied from 40 to 60 keV and optical depth τ from 2.3 to 3.4. For the high-energy power-law component above 300 keV, seen more prominently in the VP spectra shown in Figure 3-a,b (VPs 36.7, 37, 38, 39, 40, 41 and 42), the best-fit photon index varied from ~ 1 in VP-42, to ~ 3.8 in VP-39. Details shown in Figure 3-a,b also include:

- Panel 2 shows the weighted averaged spectrum measured by four BATSE LADs (LADs 0, 2 4 & 6) during VP-36.5 (TJD 8847-8853), the 1st local high-energy flux minimum described in Section 3.1-B (see also Figure 1). The solid line is the best-fit Compton model with $kT = 42.2$ keV and $\tau = 3.52$ to the four "source-viewing" LAD-spectra (LADs 0, 2, 4, & 6). The reduced χ^2 for the fit is 1.38 for 53 degrees of freedom. Shown also in this panel is a comparison of the BATSE spectrum with those measured simultaneously by OSSE (retrieved from the OSSE archive in 1995; see also Ling et al. 2000) and COMPTEL (van Dijk et al. 1995). Below 429 keV, OSSE fluxes were generally lower than those of BATSE by ~ 5 -25%. Above 429 keV, upper limits measured by BATSE are consistent with the positive fluxes in the 518-678 keV bin measured by OSSE, and in the 750-1000 keV and 1000-2000 keV bins measured by COMPTEL (van Dijk et al 1995). The high-energy fluxes measured by COMPTEL and OSSE in this period were lower than those measured by BATSE in VP-35 (e.g.by approximately a factor of two at 1 MeV. They provide, however, an important confirmation of the high-energy component of the two-component (Compton and power law) spectrum observed by BATSE in VP-35, and further suggest that such component is variable.

- The high-energy component >300 keV was also clearly visible in the four VP spectra that follow (Figure 3-a,b-panels 3-6: VP-37, 38, 39 and 40) covering the period from TJD 8855 to TJD 8902. The power-law indices for these four spectra vary from

2.7 to 3.8. The two larger indices of 3.44 and 3.89 for VP-37 and VP-39, respectively, correspond to the 1st (between "a" and "d") and 2nd (between "d" and "e") minimum of the high-energy flux shown in Figure 1 panels 5 & 6. None of these VP spectra can be adequately fitted with a single-component Compton model (solid line). The reduced χ^2 for fitting these spectra varies from ~ 2.5 to ~ 8.4 . The reasons for the poor fit are: (1) the presence of the high-energy flux above 300 keV in the spectrum, and (2) short-term (single-day) spectral changes shown in Figure 2, due possibly to intrinsic changes in the system, preclude any possibility for a simple model (e.g. Compton model) to adequately fit the long-term VP spectrum. For three of the four VP spectra (VP-37, 38 and 40) in which high-energy fluxes are prominently visible, data measured by all "source-viewing" LADs were display for demonstrating their consistency. The dashed line in each panel represents the best-fit power law to the fluxes measured by all "source-viewing" LADs in the five high-energy channels (313 - 1700 keV). Differences in spectral indices among the VP spectra reflect variability in the high-energy fluxes observed during this period. A relatively hard high-energy component was seen in the VP-38 and VP-40 spectra with indices of 2.65 and 2.87, respectively. They correspond to the 2nd and 3rd sub-maxima shown in panels 5 & 6 in Figure 1. Included in Figure 3-a,b panels 3 & 5 are also simultaneous OSSE VP-37 and VP-39 spectra, respectively, extracted from the OSSE unpublished archive in 1995 (Ling et al. 2000). Again, the OSSE fluxes are systematically lower than those of BATSE below 500 keV by few to 26% in VP-39, and 25-47% in VP-37. More significantly, the weighted averaged VP-37 fluxes in energy bins of 766-1104 keV and 1104-1700 keV of $(3.35 \pm 1.82) \cdot 10^{-6}$ and $(1.52 \pm 0.81) \cdot 10^{-6}$ photons/cm²-s-keV measured by BATSE are higher than the OSSE 3σ upper limits of $\sim 9 \cdot 10^{-7}$ and $8 \cdot 10^{-7}$ in energy bins 887 - 1160 keV and 1160-1517 keV, respectively. The reason for the discrepancy is not known at this time. Since individual OSSE VP spectrum has not been published in open literature, such discrepancy are therefore not formally confirmed. Finally, no high-energy flux was observed

inVP-41, which corresponds to the 3rd minimum (between "e" and "f") shown in Figure 1 panel 5 & 6.

- The hardest high-energy component was seen in the VP-42 spectrum with a power-law index of ~ 1 . Positive fluxes were measured in each of the five high-energy channels (313-429 keV, 429-595 keV, 595-766 keV, 766-1104 keV and 1104-1700 keV) at 13.8, 7.9, 6.2, 5.7, and 6.7σ significance, respectively. Furthermore, they were consistently seen by the two "source-viewing" LADs (5 & 7). The difference of the fluxes in each energy band measured by the two LADs was estimated to be 1.1, 0.8, 2.0, 0.4, and 0.2σ significance. Such hard MeV component reminds us of the MeV "bump" seen in the γ_1 spectrum of Cygnus X-1 (Ling et al. 1987).

c. Figure 4 shows a comparison of spectra measured simultaneously by BATSE and SIGMA (Roques et al 1994) during the period from TJD 8850 to TJD 8891. Above 300 keV, BATSE results were consistent with those of SIGMA. Below 300 keV, SIGMA results were generally lower by $\sim 20\%$ at 50 keV, $\sim 33\%$ at 100 keV and $\sim 43\%$ at 200 keV. Since the source fluxes were highly variable during this 40-day period, part of the discrepancy below 300 keV may be due to differences in weighting the short-term daily fluxes in deriving the averaged spectrum.

3.2.2. *Low-State Spectrum*

When the 35-500 keV luminosity dropped below to 20% of the peak value observed on TJD 8848 (see Table 1) after TJD 8925, the source spectrum returned to a power law with indices of $\sim 1.8-2$ (see Figure 2 panels 28-36), similar to that first seen at the start of the event on TJD 8839. Figure 5 shows a comparison of a 30-day averaged low-state spectrum observed on TJD 9010-9040 with the average high-state spectrum covering the six periods

shown in Figure 3 from TJD 8841 to TJD 8865 (VPs 35-38). The two spectra are clearly distinct. Above 300 keV, the low-state spectrum with a power index of ~ 2 is harder than that of the high-state spectrum with index of ~ 5.2 , and intersects the latter at ~ 600 keV. Similar spectral features and characteristic were also observed in Cygnus X-1 between the x-ray low-state and high-state spectra (McConnell et al. 2002).

4. Discussion

A comprehensive study of the long-term spectral and temporal properties of soft gamma-ray emission of GROJ0422+32 shown in the 1992 outburst is the primary subject of this report. Highlights of our results are as follows:

- The light curves in the six energy bands (Figure 1) show that the high-energy (>200 keV) flux led the low-energy flux (<200 keV) by ~ 5 days in reaching the initial peak, but lagged the latter by ~ 7 days before starting to decline.
- We confirm the secondary maximum in the low-energy (<200 keV) flux at \sim TJD 8970-8981, ~ 120 days after the first maximum, as reported earlier by the BATSE team (Harmon et al. 1993). Such a secondary maximum was also prominently observed in the 200-300 keV band, but became less pronounced at higher energies (Figure 1). We also observed a dip in intensity in all six energy-bands at \sim TJDs 8973-8977 in the midst of the secondary maximum. The dip is similar to that seen during the primary peak ~ 120 days earlier.
- During this 200-day period, the spectrum evolved from the low intensity power-law shape with photon index of 1.75 on TJD 8839, to a high-intensity shape of two components: a thermal-Comptonization shape below 300 keV, with a power-law tail above 300 keV with variable index from ~ 1 to ~ 4 (Figures 2 & 3).

- The spectrum remained roughly in this two-component shape until ~ 9 November (TJD 8935) when the 35-429 keV luminosity dropped to $\sim 20\%$ of its peak value observed on TJD-8848. At that time, the spectrum returned to the initial power-law shape with an index of ~ 2 and stayed in this shape until the end of the event (Figures 2 & 3; Table 1).

- Strong episodes of high-energy (400-1000 keV) emission were observed on four separate occasions during the first 84 days of the event (Figure 1 panels 5-6). This corresponds to 0-0.70 phase of the 120-day period, which was first suggested by Iyudin & Haberl (2001) based on several years of COMPTEL observations. COMPTEL results showed that the 1.5-2 MeV emission was primarily confined to 0-0.5 phase of the 120-day period

- The averaged high-intensity spectrum above 300 keV obtained on TJD 8841-8865 is softer than the average low-intensity power-law spectrum (TJD 9010-9040), and intercepts the latter at ~ 600 keV (Figure 5).

- Several key features displayed by GROJ0422+32 spectra are remarkably similar to those seen in Cygnus X-1 suggesting that similar processes may be at work in both systems. A direct comparison of these features is shown in Table 2:

The two-component Compton plus power-law spectrum observed in GROJ0422+32, Cygnus X-1 and several other BH binaries has been the subject of several theoretical studies in recent years. Earlier works in interpreting the Cygnus X-1 spectra below ~ 1 MeV in terms of a two-region core/corona thermal model (Ling et al. 1997; Skibo & Dermer 1994) using the Monte Carlo approach, have had some degree of success. However, we have now seen persistent power-law emission extended to ~ 1 MeV in both the high and low-intensity γ -ray state spectra of GROJ0422+32 as shown in this and other papers (Grove et al. 1998; Van Dijk et al. 1995; Iyudin & Habert, 2001), and in the γ_0 (high/soft) and γ_2 (low/hard) spectra of Cygnus X-1 (Ling et al. 1997; McConnell et al. 2000, 2002). These results suggest that the high-energy power-law component cannot be adequately

interpreted in terms of pure thermal processes alone, and that non-thermal processes must be also at work in these systems. Power-law spectral tail may be associated with dynamical Comptonization processes in converging flows onto a black hole (Laurent & Titarchuk 1999; Turolla et al. 2002). Turolla et al. (2002) showed that a power-law photon index of <3 can be produced by up-scattering of primary photons off in-falling electrons. However, no direct comparison between theoretical predictions and observational data can be obtained at this time. Non-thermal gamma-ray emission may be also associated with jets, which was discussed by Meier (2001) as a natural consequence of accretion flows onto rotating black holes. A relativistic jet in Cygnus X-1 has been observed in the radio band (Stirling et al. 1996; Fender et al. 2000; Fender 2001) when the source was in the γ_2 (low/hard) state. Radio emission was also seen in GROJ0422+32 (Shrader et al. 1994), although no jet-like structure was resolved from these observations. A more general approach using a hybrid thermal/non-thermal comptonization model (EQPAIR) was proposed by Coppi (1998) (see also Gierlinski et al., 1999). In this model, the electron distribution consists of a Maxwellian component with a temperature, kT , plus a non-thermal power-law component. The acceleration of non-thermal electrons is independently taking place but is coupled to the background thermal plasma by Compton scattering and Coulomb collision processes. The model basically allows for both thermal and nonthermal comptonization of soft photons, as well as pair production, Compton reflection, and bremsstrahlung emission. Although we do not know with certainty at the present the processes for producing the non-thermal power-law γ -ray emission (e.g. jets or other processes), our data suggest that non-thermal power law emission was present throughout the outburst. It was fully visible in the 35 keV to 1 MeV energy band when the GROJ0422+32 was in the low-intensity state, and only partially visible in the 313 - 1 MeV band when it was in the high-intensity state. Furthermore, the average spectral index for the former was harder (~ 2) than the latter (~ 3 -5). We suggest a possible scenario for interpreting the observed data that includes a

separate non-thermal (perhaps a jet-like) source region in the ADAF model of Esin et al (1998) along with the source geometry envisioned by Poutanen & Coppi (1998) and others (Coppi 1998; Fender & Kuulkers 2001; Zdziarski 2002) (see Figure 6). In this scenario, during the high-intensity state (or γ_2 state for Cygnus X-1; Figure 6 right panel), the system consists of a hot inner corona, a cooler outer thin disk, and a region that produced the variable power-law γ -ray emission. Under this condition, the transition radius of the disk is ~ 100 Schwarzschild radii from the black hole. Electrons in the hot corona up-scattered the low-energy photons produced both inside the corona as well as from the outer disk to form the Comptonized component that dominates the spectrum in the 35-300 keV range. They also down-scattered the high energy photons (>10 MeV) produced in the "jet" region resulted in forming a softer power-law component observed in the 300 keV to 1 MeV range compared to that observed in the low-intensity spectrum.

When the source was in the low-intensity soft γ -ray state (or γ_0 state for Cygnus X-1) due probably to a significantly increase of the accretion rate, a large soft flux was produced in the disk that effectively quench and cool the inner corona, and moved the transition radius inward to a distance very close to the horizon (Figure 6 left panel). Under this condition, the Comptonized component in the 35-300 keV range diminishes, and the source spectrum is dominated by the unperturbed power-law emission produced in the "jet"-like non-thermal source γ region with a characteristic index of ~ 2 .

While the above scenario helps to interpret some aspects of the new observational features, there are several issues that are not yet resolved: (1) what is the cause for the time-lag effect of \sim few days seen between the low (<200 keV) and high-energy (>200 keV) photons? Is this an indication of the response time for the Comptonization process in the system to a sudden change of the accretion rate? (2) The hard high-energy (0.3-1 MeV) spectral component observed in VP-42 with an index of ~ 1 is strongly reminiscent of the

”MeV bump” seen in the γ_1 spectrum of Cygnus X-1 (Ling et al. 1987). Is this caused by a intrinsic change in the non-thermal emission, or is it a signature of the pair plasma (Liang and Dermer 1988; Ling & Wheaton 1989; Poutanen & Coppi, 1998) produced by the heating the corona to very high temperature ($\sim 10^9$ K). Such heating could be caused by a further reduction of the accretion rate that led to the reduction of soft photons for its cooling? (3) The intensity of the radio emission was observed to track the gamma rays throughout the outburst for GROJ0422+32 (Shrader et al. 1994), but was only seen in the γ_2 state (and not the γ_0 state) of Cygnus X-1 (Stirling et al. 1996; Fender et al. 2000; Fender 2001). What is the reason for this difference? Is it caused by a difference of the ”beaming” effect in the two systems? We hope these results will stimulate further theoretical and observational investigations in the future of this very unusual and exciting black-hole system discovered by BATSE.

We wish to thank Gerald Fishman, Alan Harmon, Mark Finger and Geoff Pendleton of the BATSE team for their support of the BATSE Earth Occultation investigation effort at JPL through-out the years, Dave Meier and Paolo Coppi for their extremely useful comments on the interpretation of these data, and undergraduate students Robert Kern, Zachary Medin, and Juan Estrella for processing the data. The work described in this paper was carried out by the Jet Propulsion Laboratory, under the contract with the National Aeronautics and Space Administration.

REFERENCES

- Arnaud, K. A., 1996, in ASP Conf. Proc. 101, *Astronomical Data Analysis Software and Systems V*, ed. G. Jacoby & J. Barnes (San Francisco; ASP), 17.
- Bonnet-Bidaud, J. M. and Mouchet, M., 1995, *A&A*, L69.
- Callanan, P. J., Garcia, M. R., McClintock, J. E., Zhao, P., Remillard, R. A., & Haberl, F. 1996, *ApJ*, 461, 351.
- Casares, J., Martin, A. C., Charles, P. A., Martin, E. L., Rebolo, R., Harlaftis, E. T., & Castro-Tirado, A. J. 1995, *MBRAS*, 276, L35-L39.
- Castro-Tirado, A. J., Pavlenko, E. P., Shlyapnikov, A. A., Gershberg, R., Hayrapetyan, V., Brandt, S., & Lund, N. 1992, *IAU Circ.* 5588.
- Castro-Tirado, A. J., Pavlenko, E. P., Shlyapnikov, A. A., Brandt, S., Lund, N., & Ortiz, J. L. 1993, *A&A*, 276, L37.
- Chevalier, C., and Ilovaisky, S. A., 1995, *A&A*, 297, 103.
- Chevalier, C., and Ilovaisky, S. A., 1996, *A&A*, 312, 105.
- Coppi, P. S., 1998, "The Physics of Hybrid Thermal/Non-thermal Plasmas" in *High energy Processes in Accreting Black Holes*, eds. J. Poutanen and R. Svensson, ASP Conf. Series, Vol. 161, p. 375 (astro-ph/9903158)
- Esin, A. A., Narayan, R., Cui, W., Grove, J. E., & Zhang, S., 1998, *ApJ*, 505, 854.
- Fender, R. P., Pooley, G.G., Durouchoux, P., Tilanus, R. P. J., and Brocksopp, C., 2000, *MNRAS*, 312, 851.
- Fender, R. P., 2001, *MNRAS*, 322, 31.
- Fender, R. P., and Kuulkers, E., 2001, *MNRAS*, 324, 923.
- Filippenko, A. V., Matheson, T., & Ho, L. C., 1995, *ApJ*, 55, 614..

- Fishman, G. J., et al. 1989, in Proc. Gamma Ray Observatory Science Workshop, ed. W. Johnson (Greenbelt: GSFC), 2.
- Garcia, M. R., Callanan, P. J., McClintock, J. E., & Zhao, P. 1996, ApJ, 460, 932.
- Gierlinski, M., Zdziarski, A. A., Poutanen, J., Coppi, P. S. Ebisawa, K., and Johnson, W. N. 1999, MNRAS, 309, 496.
- Grove, J. E., et al., 1994, AIP Conference Proceedings 304, Second Compton Gamma-Ray Observatory Symposium, ed. C. E. Fichtel, N. Gehrels, and J. P. Norris (New York:AIP), 192.
- Grove, J. E., Johnson, W. N., Kroeger, R. A., McNaron-Brown, K., Skibo, J. G., and Philips, B. F., 1998, ApJ, 500, 899.
- Harmon, B. A., et al. 1992, IAU Circ. 5584.
- Harmon, B. A., et al. 1993, in AIP Conf. Proc. 280, Compton Gamma Ray Observatory Symp., ed. M. Friedlander, N. Gehrels, & D. Macomb (New York: AIP), 314,
- Harmon, B. A., et al. 1994, in 2nd Compton Symp., ed. C. E. Fichtel, N. Gehrels, and J.P. Norris (New York:AIP), 210.
- Harmon, B. A., Fishman, G. J., Wilson, C. A., Paciesas, W. S., Zhang, S. N., Finger, M. H., Koshut, T. M., McCollough, M. L., Robinson, C. R., and Rubin, B. C. 2002, ApJS, 1, 149.
- Iyudin, A. F., and Haberl, F., 2001, in AIP Conf. Proc. 280, Gamma-Ray Astrophysics 2001 Symp., ed. S. Ritz, N. Gehrels, & C. R. Shrader (New York: AIP), 116.
- Kouveliotou, C., et al., 1993, in AIPConf. Proc. 280, Compton Gamma-Ray Observatory, St. Louis, ed. M. Friedlander, N. Gehrels, & D. Macomb (New York: AIP), 319,
- Kouveliotou, C., 1994, in 2nd Compton Symp., ed. C. E. Fichtel, N. Gehrels, and J. P. Norris (New York:AIP), 202.

- Laurent, P., and Titarchuk, L., 1999, *ApJ*, 511, 289.
- Liang, E.P, and Dermer, C. D., 1988 , *ApJ* , 325 (2), L39.
- Ling, J. C., 2001, in *AIP Conf. Proc.* 280, *Gamma-Ray Astrophysics 2001 Symp.* ed. S. Ritz, N. Gehrels, and C. R. Shrader (New York: AIP), 135.
- Ling, J. C., Mahoney, w. A., Wheaton, W. A., amd Jaconsen, A. S. 1987, *ApJ*, 321, L117.
- Ling, J. C., and Wheaton, W. A., 1989, *ApJ*, 343, L57.
- Ling, J. C., Wheaton, W. A., Mahoney, W. A., Skelton, R. T., Radocinski, R. G., and Wallyn, P. 1996, *A&AS*, 120, 667.
- Ling, J. C., et al. 1997, *ApJ*, 484, 375
- Ling, J. C., et al. 2000, *ApJS*, 127, 79
- Maisack, M., et al. 1994, in *2nd Compton Symp.*, ed. C. E. Fichtel, N. Gehrels, and J. P.Norris (New York:AIP), 346.
- McConnell, M. L., et al. 2000, *ApJ*, 543, 928.
- McConnell, M. L., et al. 2002, *ApJ*, 572,: 984.
- Meier, D. L., 2001, *ApJ*, 548, L9.
- Orosz, J. A., and Bailyn, C. D. 1995, *ApJ*, 446, L59.
- Paciesas, W. S., et al. 1992, *IAU Circ.* 5580.
- Phlips, B., et al., 1996, *ApJ*, 465, 907.
- Pietsch, W. et al. 1993, *A&A*, 273, L11.
- Poutanen, J. & Coppi, P. S. 1998, *Physica Scripta*, T77, 57 (astro-ph/9711316).
- Roques, J. P., et al. 1994, *ApJS*, 92, 451
- Shrader, C. et al., 1992a, *IAU Circ.* 5580.

- Shrader, C., Wagner, R. M., Starrfield, S. G., Hjellming, R. M., Han, X. H., 1992b, in 1st Compton Symp., ed. M. Friedlander, N. Gehrels, & D. J. Macomb (New York:AIP 280), 324.
- Shrader, C. R., Wagner, R. M., Hjellming, R. M., Han, X. H., & Starrfield, S. G.1994, ApJ, 434, 698.1994, ApJ, 434, 698.
- Skibo, J.G. and Dermer, C.D., 1995, Ap. J. 455, L25.
- Stirling, A. M., Spencer, R. E., de la Force, C. J., Garrett, M. A., Fender, R. P., and Ogley, R. N., 2001, MNRAS, submitted or astro-ph/0107192.
- Sunyaev, R. A., & Trumper, J. 1979, Nature, 279, 506.
- Sunyaev , R. A., & Titarchuk, L. G., 1980, A&A, 86, 121.
- Sunyaev , R. A., et al. 1991, A&A, 247, L29.
- Sunyaev, R. A., et al. 1993, A&A, 280, L1
- Turolla, R., Zane, S., & Titarchuk, L., 2002, ApJ, 576, 349.
- Van der Hooft, F., et al. 1999, ApJ, 513, 477.
- Van der Klis, M., 1994, ApJS, 92,511.
- Van Dijk, R., et al. 1995, A&A, 296, L33.
- van Paradijs , J., & McClintock , J. E. 1995, in X-Ray Binaries, ed. W. H. G. Lewin, J.van Paradijs, & E. P. J. van den Heuvel (Cambridge: Cambridge Univ. Press), 58.
- Vikhlinin, A., et al. 1995, ApJ, 441, 779.
- Wagner, R. M., Bertram, R., Starrfield, S. G., & Shrader, C. R. 1992, IAU Circ. No.5589.
- Wallyn , P., Ling, J. C., Mahoney, W. A., Wheaton, W. A., Durouchoux, P., 2001, ApJ, 559, 342.

Zdziarski, A.A., Poutanen, J., Paciesas, W. S., and Wen, L., 2002, submitted to Ap.
J.(astro-ph/0204135).

Zhang, S. N. et al., 1997, ApJ 477, L95.

FIGURE CAPTIONS

Fig. 1.— Flux histories, with 1-day resolution, in six separate energy-bands are shown. The high-energy (see panels 3-6) flux rose more sharply and reached the first of the four episodic peaks (shown by four vertical dashed lines "a", "d", "e" and "f") on TJD 8843 ("a") five days before the first low-energy sub-peak (vertical dashed line "b") on TJD 8848. The decrease of the low-energy flux between the first and the second sub-peaks on TJD 8855 (vertical dashed line "c") is only $\sim 4\%$. However, the decrease of the high-energy fluxes (3rd to 6th panels) between its first and second sub-peak on TJD 8862 (vertical dashed line "d") is significantly more pronounced. The high-energy fluxes also lagged the low-energy fluxes in starting the decline phase by ~ 7 days (see vertical dashed lines "c" and "d"). A broad "secondary maximum" for the low-energy fluxes ~ 120 days later at \sim TJD 8970-8981 which was observed and reported by the BATSE team earlier (Harmon et al. 1993) was also prominently observed in the 200-300 keV bin, but became less pronounced at higher energies. Note that there is also evidence for a "dip" in intensity at around TJD 8977 in the midst of the "secondary maximum" which is shown in all six energy bands.

Fig. 2.— (a) A sample of 9 single-day spectra was selected to show the evolutionary changes of the source spectrum during the first twelve days (TJD 8839-8850) of the 200-day event (see also Figure 1). The spectrum evolved from the "low-intensity" power-law shape at the onset on TJD 8839 to a "high-intensity" Comptonized shape <300 keV two days later on TJD 8841. A high-energy power-law component >300 keV was also observed prominently in the VP-35 spectra shown in Figure 3a during the first of the four "episodic" γ -ray emission periods. However, it was not clearly visible in the single-day spectra due to statistical limitation of the data. Note that in three panels of the middle column, spectra measured simultaneously by all "source viewing" LADs on that day are shown and compared. This is a self imposed consistent test to serve as "quality control" to ensure credibility of all EBOP results. (b)

A second set of 9 single-day spectra covering the period TJD 8851-8862 (identified as "10" to "18" in Figure 1) During this period, the fluxes, specifically those >200 keV, gradually rose from a local minimum at \sim TJD 8850 to a peak at \sim TJD 8862. While the spectrum averaged over the entire period (VP-37, see Figure 3c) remained in the same two-component shape, namely a Comptonized component <300 keV followed by a variable power-law >300 keV that was visible even in the single-day spectra on TJD 8858, 8859 and 8862 (panels 16-18), respectively. (c) A third set of 9 single-day spectra covering the period TJD 8863-8945 (identified as "19" to "27" in Figure 1). During this period, the spectrum remained approximately in the same two-component shape (see also Figure 3-a,b panels 4-8), namely a Comptonized component below 300 keV and a variable power-law >300 keV, until \sim TJD 8935 when the 35-429 keV luminosity dropped to $\sim 20\%$ of the peak value (see also Table 1). The spectrum then returned to the initial power law shape as that shown on TJD 8839 (Figure 2a panel 1) with index of ~ 2 (see panels 26 & 27). (d) A fourth set of 9 single-day spectra covering the period TJD 8955-9033(identified as "28" to "36" in Figure 1). The spectrum stayed in the power law shape throughout this period until the end of the event.

Fig. 3.— (a) Four consecutive VP (Viewing Periods 35, 36.5, 37 and 38) spectra covering the initial phases of the outburst from TJD 8841 to TJD 8865. A variable high-energy (>300 keV) power-law component superposed to the Compton component below 300 keV, is clearly visible in panels 1, 3, and 4 that correspond to the two of the high-flux periods ("a" and "d") shown in Figure 1. High-energy (>400 keV) fluxes measured by COMPTEL (van Dijk et al. 1995) and OSSE (from the OSSE archive, see Ling et al. 2000) during VP-36.5 are also included in panel 2 for comparison. Shown also in panel 3 for comparison are unpublished OSSE spectra for VPs 37. OSSE fluxes below 500 keV are generally lower than those of BATSE by $\sim 25 - 47\%$ for VP-37. (b) A second group of consecutive VP (Viewing Periods 39, 40, 41 and 42) spectra covering the period from TJD 8867 to TJD 8923. During this period, two strong episodes of gamma-ray emission were seen that peaked at \sim TJD 8889 (see

Figure 1 "e") and TJD 8919 (see Figure 1 "f"), respectively. A strong variable high-energy (>300 keV) spectral component superposed to the Compton component below 300 keV, is clearly visible in the corresponding VP-40 and VP-42 spectra. OSSE unpublished spectrum for VP- 39 (from OSSE archive, see Ling et al. 2000) respectively is also included in panel 7 for comparison. They are generally lower than those of BATSE by few-26%. The strong 400-1700 keV fluxes that were consistently measured by the two "source viewing" LADs (5 & 7) in VP-42 with a power-law index of ~ 1 , is reminiscent of the MeV "spectral bump" seen in the γ_1 spectrum of Cygnus X-1 (Ling et al. 1987)

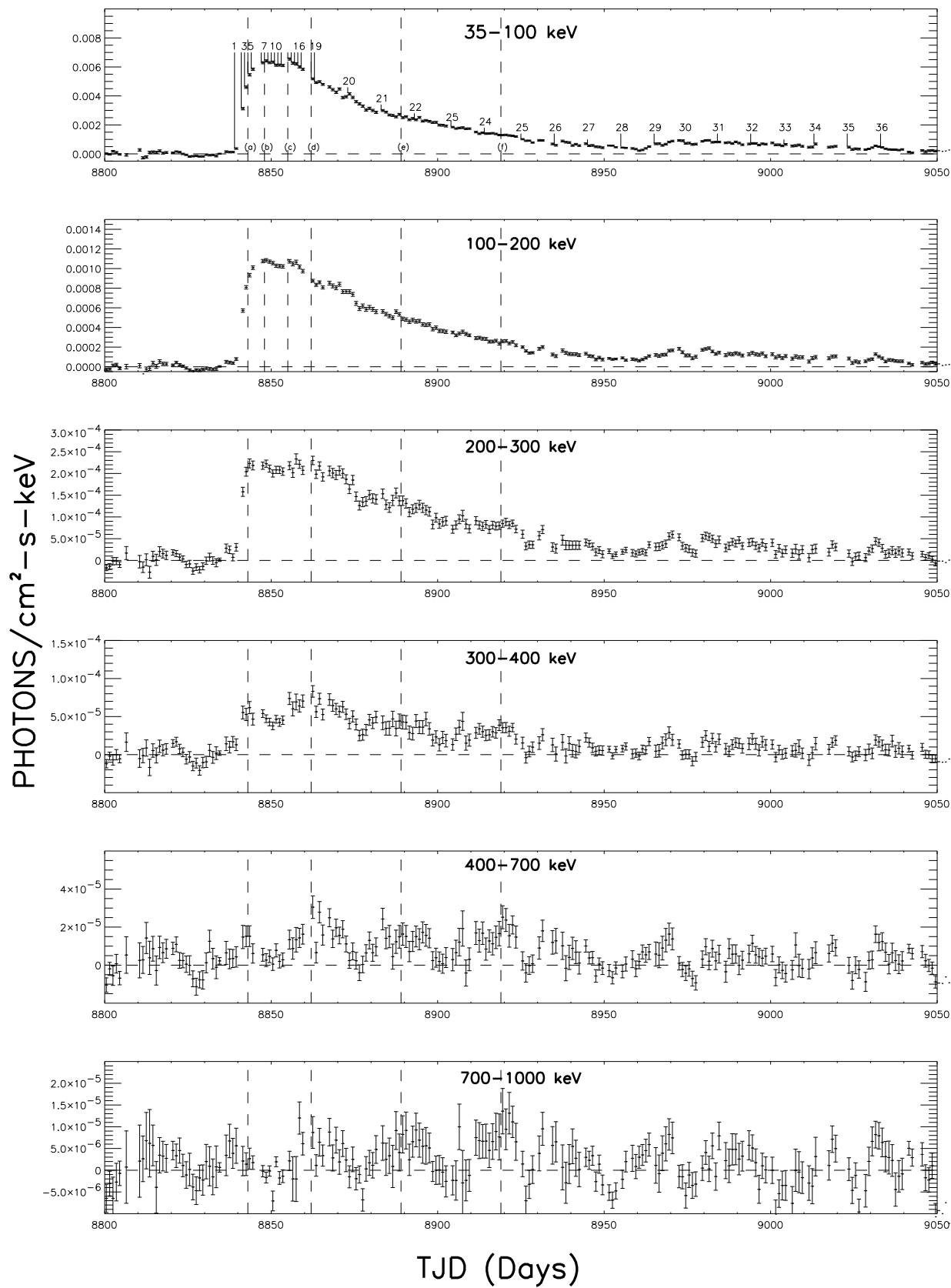
Fig. 4.— A direct comparison of the spectra measured simultaneously by BATSE and SIGMA (Roques et al.1994; E. Jourdain 2002, private communication) during a ~ 40 -day period between TJD 8850 and 8891. Above 300 keV, BATSE results were consistent with those of SIGMA. Below 300 keV, SIGMA results were generally lower by $\sim 20\%$ at 50 keV, $\sim 33\%$ at 100 keV and $\sim 43\%$ at 200 keV. The discrepancy may be due to differences in weighing the short-term variable fluxes in the long-term averages.

Fig. 5.— Averaged high-intensity spectrum (TJD 8841-8865) and low-intensity spectrum (TJD 9010-9040) have distinct shape. The former has two components: a Comptonized component below 300 keV followed by a power law (dashed line) above 300 keV, while the latter has only one, a power law. The two spectra intersect at ~ 600 keV. These features are similar to those seen in Cygnus X-1 (Ling et al. 1997; Phlips et al, 1996; McConnell et al. 2001; McConnell et al 2002) for the γ_2 and γ_0 -state spectra which intercepted at ~ 1 MeV. Such strong resemblance of the spectral properties of the two sources strongly suggests that similar processes were at work in both systems.

Fig. 6.— A simple sketch of the system by including a "jet-like" region that produced the

non-thermal gamma-ray emission in the ADAF model of Esin et al (1998) along with the source geometry envisioned by Poutanen & Coppi (1998) and others (Coppi 1998; Fender & Kuulkers 2001; Zdziarski 2002). During the "high-intensity" state (right panel), the system consists of a hot inner corona, a cooler outer thin disk, and a jet-like region that produced the variable power-law γ -ray emission. Under this condition, the transition radius of the disk is ~ 100 Schwarzschild radii from black hole. Electrons in hot corona up-scattered the low-energy photons produced both inside the corona as well as from the outer disk to form the Comptonized component observed in the 30-300 keV range. The same electrons also down-scattered the high energy power-law photons produced in the "jet" region resulted in forming a softer power-law component observed in the 300 keV to 1 MeV range compared to that observed in the "low-intensity" spectrum. During the "low-intensity" state due probably to a significantly increase of the accretion rate, a large amount of soft photons produced in the disk effectively cool and quench the corona, and moved the transition radius inward to a distance very close to the horizon (Figure 6 left panel). Under this condition, the Comptonized component in the 30-200 keV range diminishes, and the soft γ -ray spectrum is therefore dominated by the unperturbed non-thermal emission in the "jet-like" region with a characteristic power law index of ~ 2 .

GRO J0422+32



TJD (Days)
Figure 1

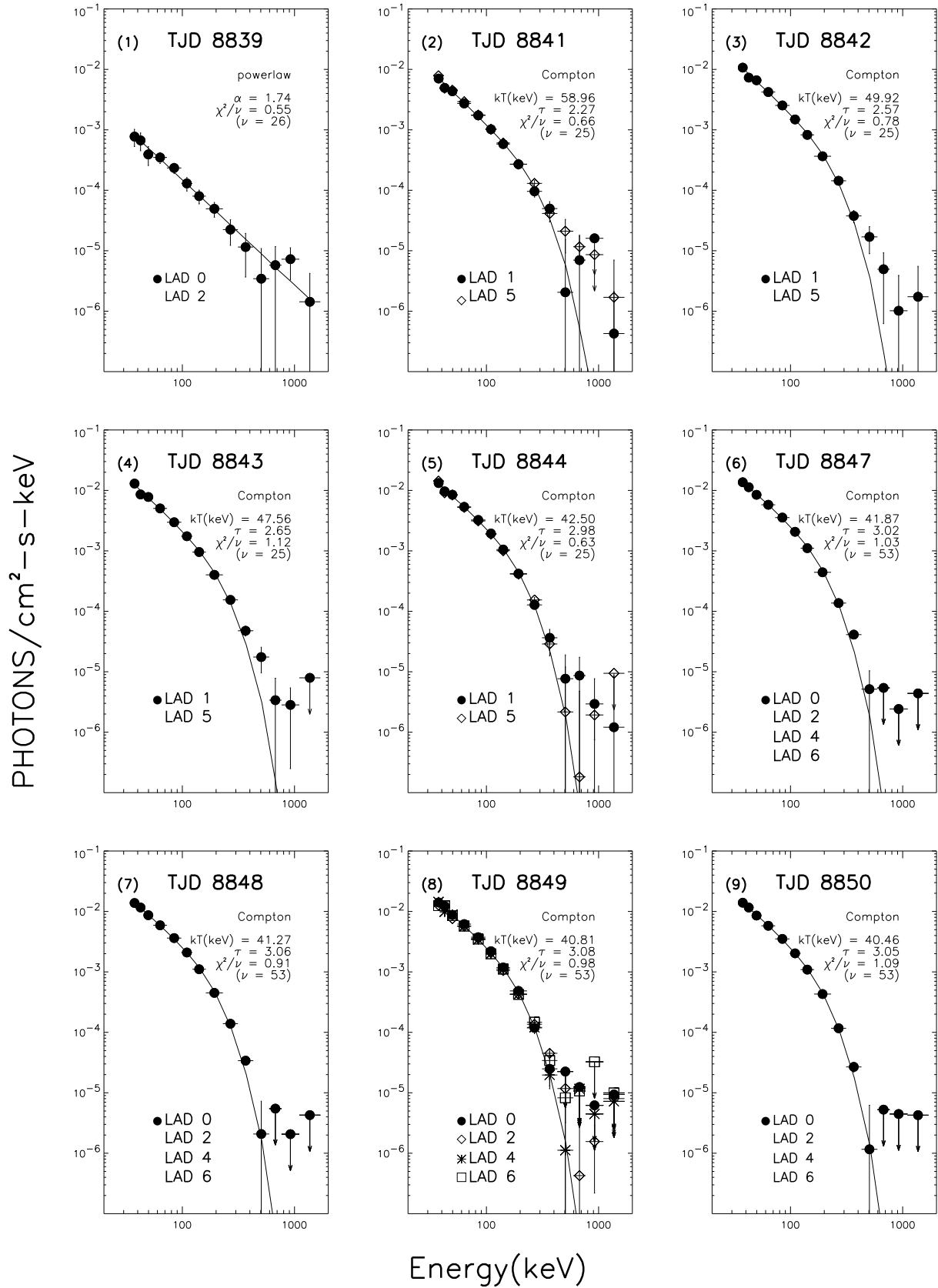


Figure 2a

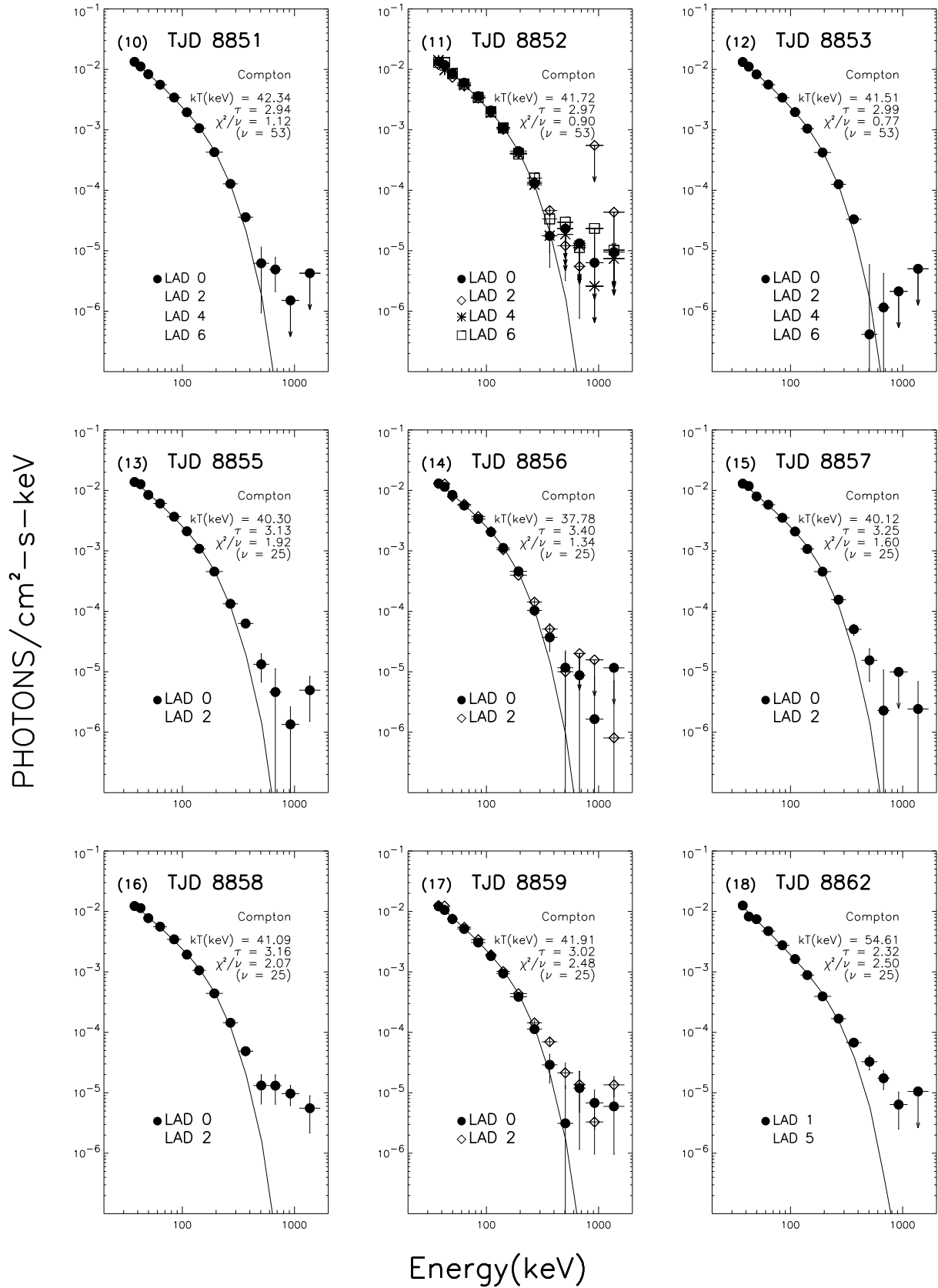


Figure 2b

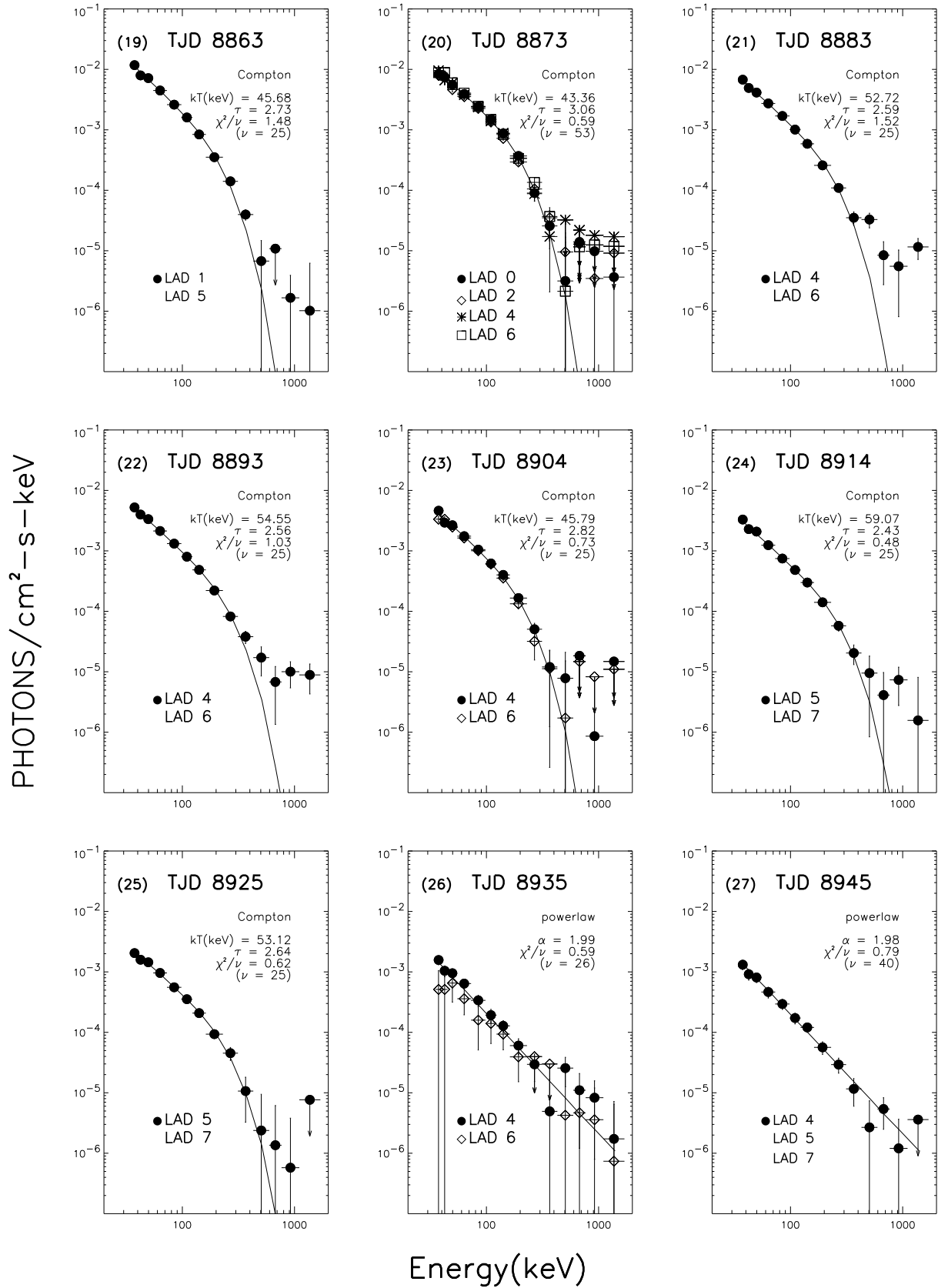


Figure 2c

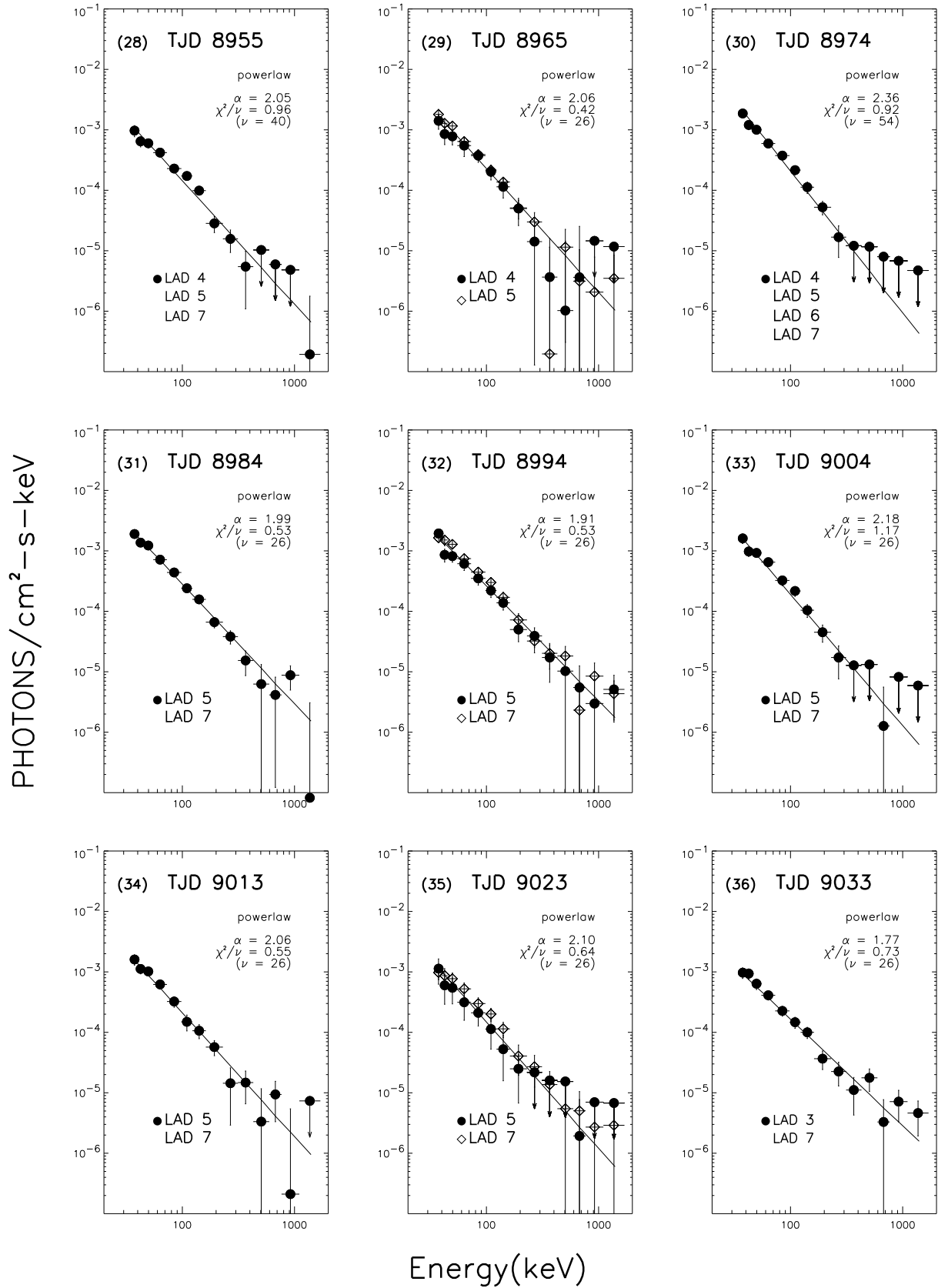


Figure 2d

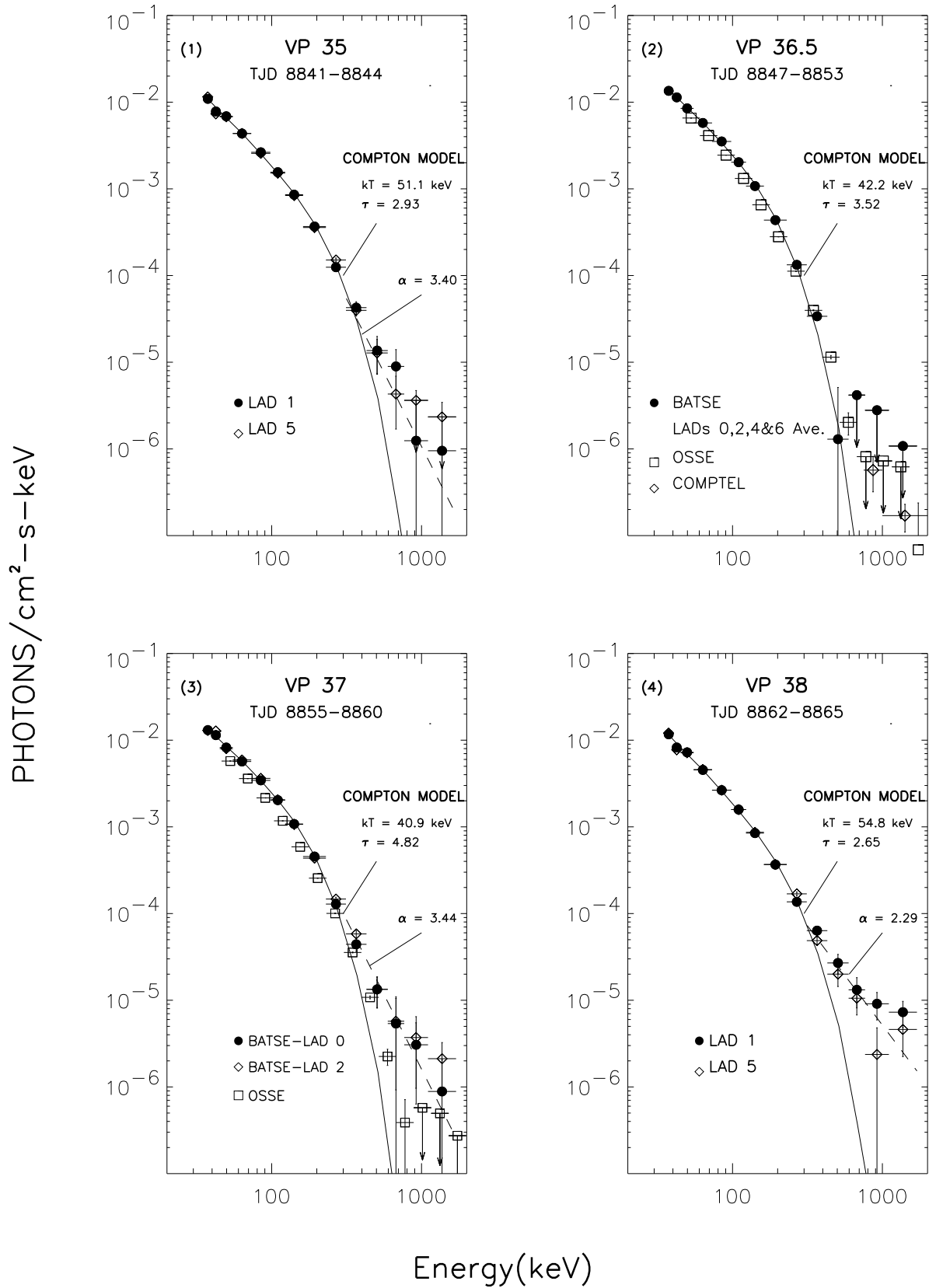


Figure 3a

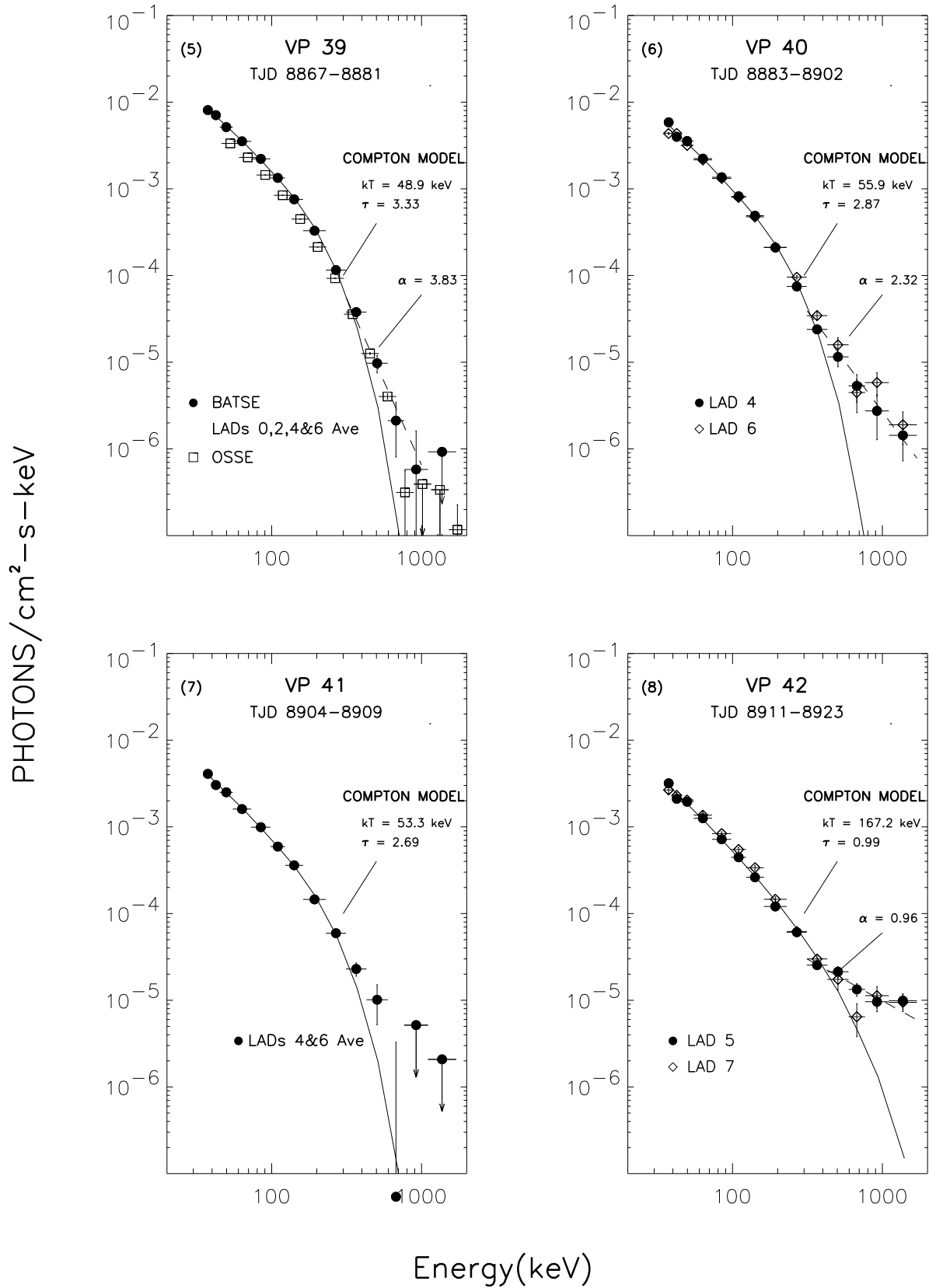


Figure 3b

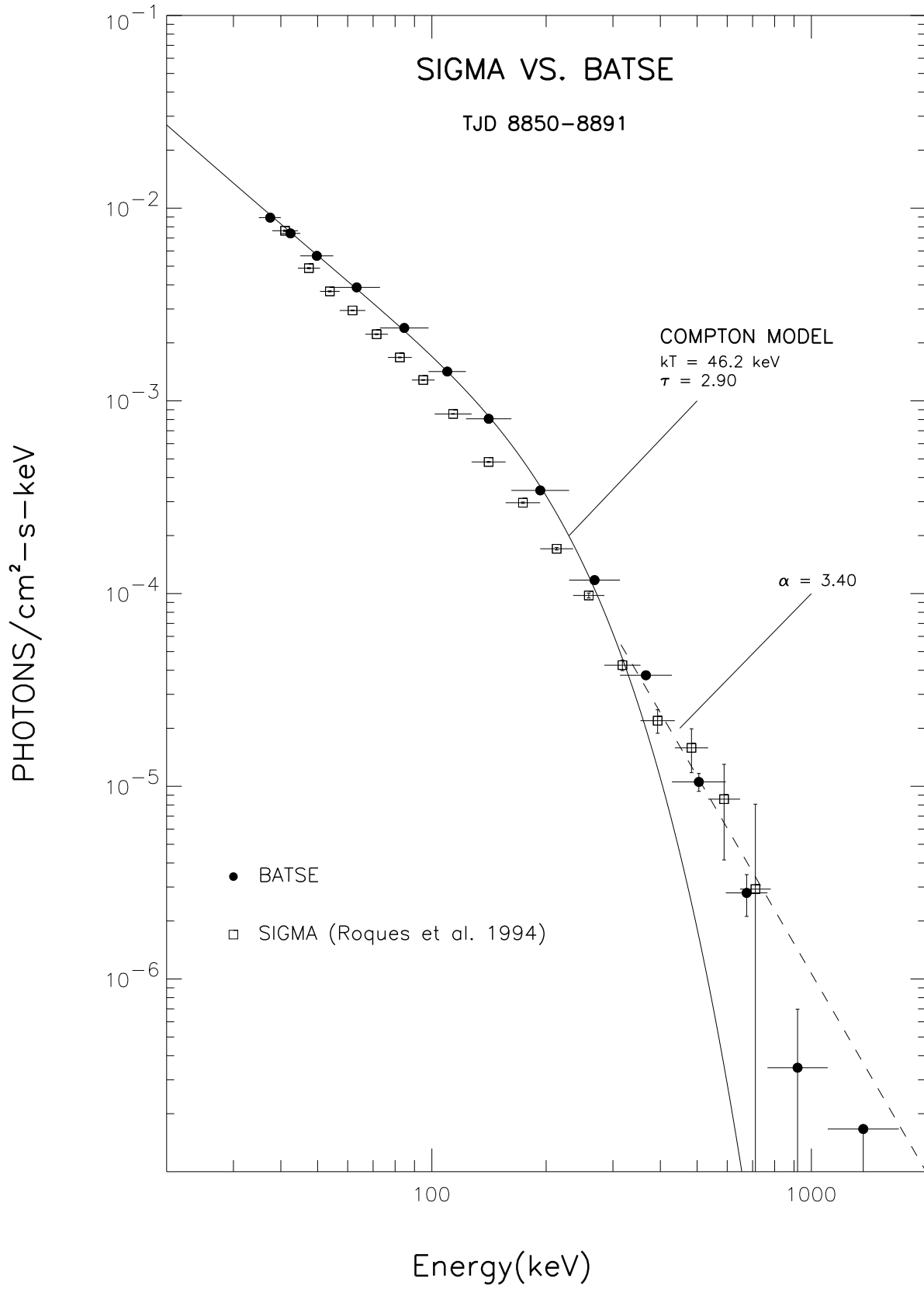


Figure 4

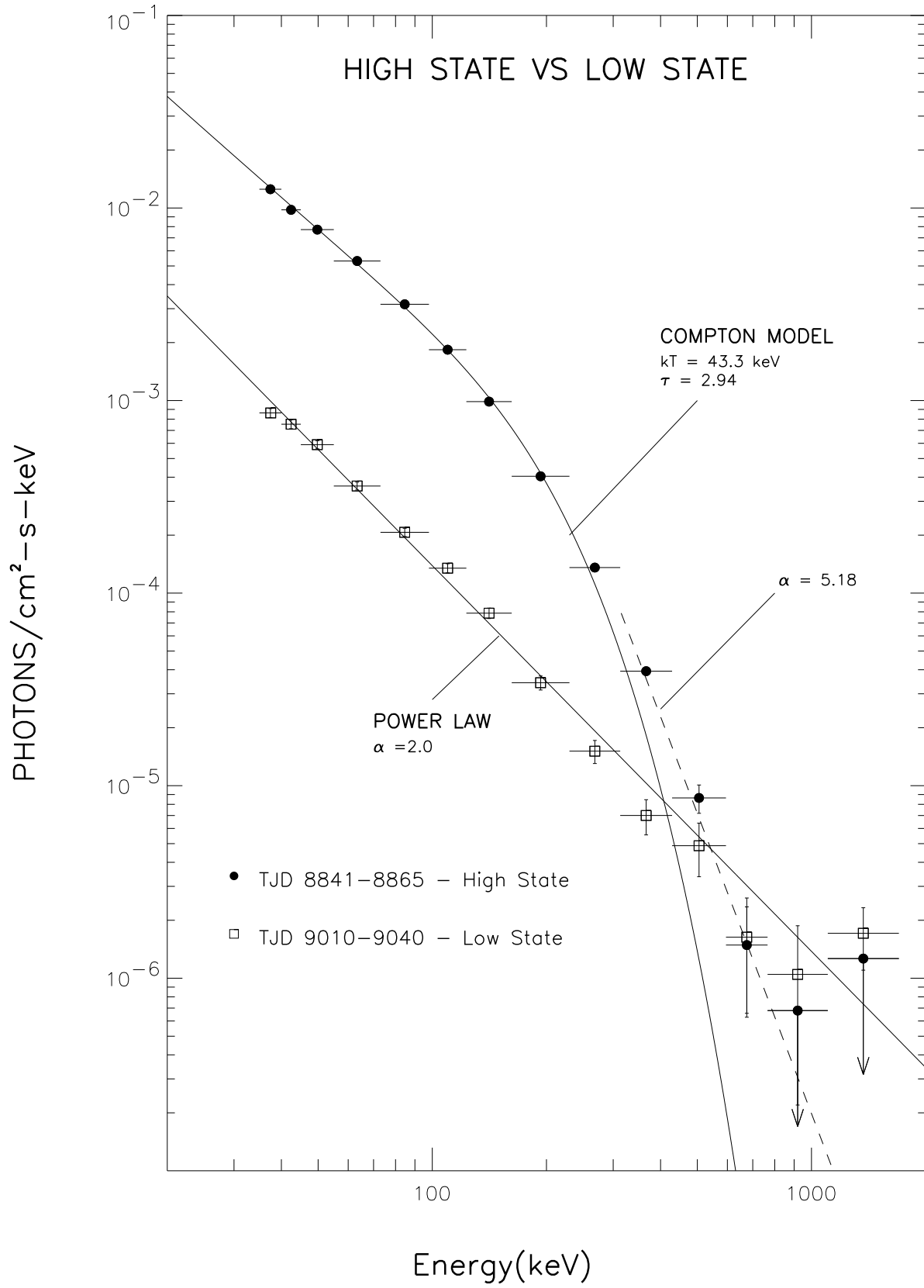


Figure 5

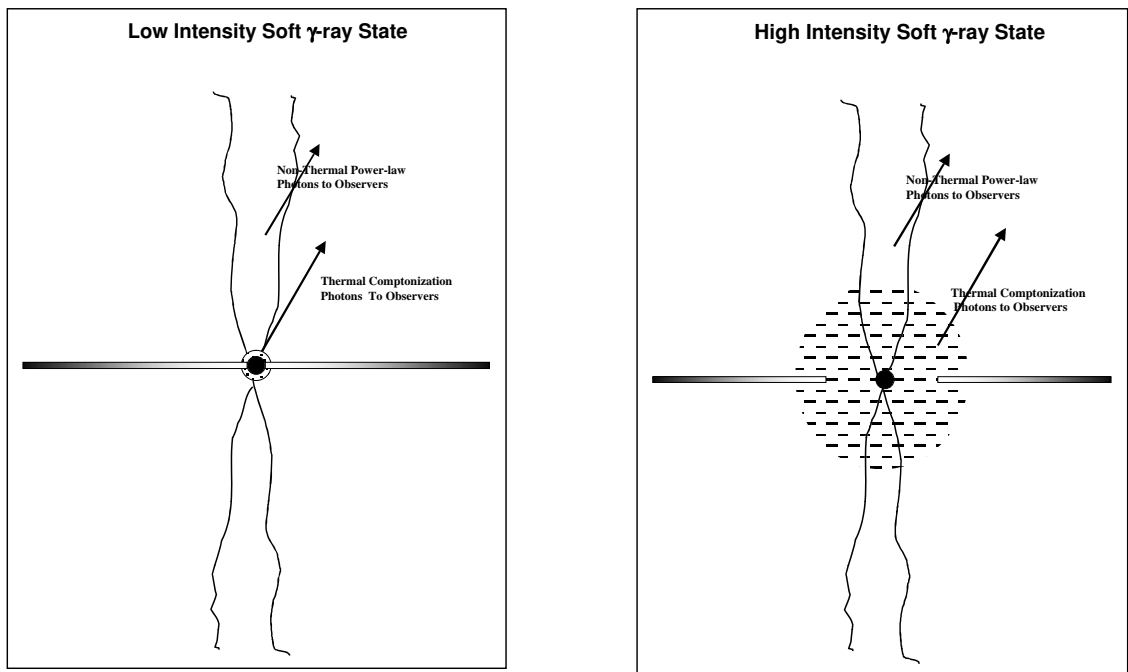


Figure 6

#	VP	TJD	LAD	FLUX 98-123 keV protons/ cm ² -s-keV (10 ⁻⁴)	Luminosity 35 - 429 keV ergs/sec (10 ³⁷) at 2.4 kpc	Power Law Model (A E ^α)			Compton Model			
						α	DOF(v)	χ ² /ν	kT (keV)	τ	DOF(v)	χ ² /ν
1	34	8839	0,2	1.30±0.33	0.42	1.74±0.13	26	0.55				
2	35	8841	1,5	10.25±0.46	2.85	2.09±.025	26	2.9	59.0±5.1	2.27±0.19	25	0.66
3	35	8842	1,5	14.87±0.46	3.93	2.13±.018	26	7.6	49.9±2.6	2.57±0.14	25	0.78
4	35	8843	1,5	17.47±0.46	4.56	2.14±.016	26	9.9	47.6±2.1	2.65±0.12	25	1.12
5	35	8844	1,5	19.19±0.47	4.74	2.16±.015	26	15.3	42.5±1.6	2.98±0.12	25	0.63
6	36.5	8847	0,2,4,6	20.69±0.41	5.09				41.9±1.2	3.02±0.11	53	1.03
7	36.5	8848	0,2,4,6	20.96±0.42	5.13				41.3±1.2	3.06±0.11	53	0.91
8	36.5	8849	0,2,4,6	20.63±0.41	5.01				40.8±1.2	3.08±0.11	53	0.98
9	36.5	8850	0,2,4,6	20.29±0.41	4.94				40.5±1.2	3.05±0.11	53	1.09
10	36.5	8851	0,2,4,6	19.55±0.41	4.88				42.3±1.3	2.94±0.11	53	1.12
11	36.5	8852	0,2,4,6	19.71±0.42	4.85				41.7±1.3	2.97±0.11	53	0.9
12	36.5	8853	0,2,4,6	19.65±0.42	4.84				41.5±1.3	2.99±0.11	53	0.77
13	37	8855	0,2	21.10±0.44	5.29				40.3±1.2	3.13±0.12	25	1.92
14	37	8856	0,2	20.82±0.48	5.02				37.8±1.3	3.40±0.14	25	1.34
15	37	8857	0,2	20.91±0.50	5.14				40.1±1.5	3.25±0.14	25	1.6
16	37	8858	0,2	19.32±0.44	4.96				41.1±1.3	3.16±0.12	25	2.08
17	37	8859	0,2	18.84±0.44	4.55				41.9±1.5	3.02±0.12	25	2.48
18	38	8862	1,5	16.31±0.40	4.19				54.6±2.6	2.32±0.11	25	2.5
19	38	8863	1,5	16.03±0.41	4.07	2.14±.016	26	10.7	45.7±1.9	2.73±0.12	25	1.48
20	39	8873	0,2,4,6	14.09±0.45	3.51	2.23±0.02	54	5.3	43.4±2.1	3.06±0.18	53	0.59
21	40	8883	4,6	10.10±0.42	2.72	2.04±0.02	26	3.73	52.7±3.8	2.59±0.19	25	1.52
22	40	8893	4,6	8.01±0.41	2.18	2.03±0.03	26	2.5	54.5±4.8	2.56±0.23	25	1.03
23	41	8904	4,6	6.14±0.30	1.47	2.11±0.03	26	3.21	45.8±4.0	2.82±0.26	25	0.73
24	42	8914	5,7	4.83±0.37	1.35	1.98±0.04	26	1.24	59.1±7.8	2.43±0.31	25	0.48
25	43	8925	5,7	3.54±0.33	0.95	1.99±0.05	26	1.4	53.1±8.5	2.64±0.41	25	0.62
26	44	8935	4,6	1.77±0.40	0.61	1.99±0.11	26	0.59				
27	201	8945	4,5,7	1.73±0.35	0.56	1.98±0.09	40	0.8				
28	202	8955	4,5,7	1.73±0.25	0.4	2.05±0.10	40	0.96				
29	203.3	8965	4,5	2.10±0.35	0.57	2.06±0.10	26	0.42				
30	203.6	8974	4,5,6,7	2.16±0.37	0.54	2.36±0.11	54	0.91				
31	204	8984	5,7	2.41±0.35	0.77	1.99±0.07	26	0.53				
32	206	8994	5,7	2.54±0.39	0.73	1.91±0.07	26	0.53				
33	207	9004	5,7	2.17±0.40	0.51	2.18±0.12	26	1.17				
34	207	9013	5,7	1.49±0.44	0.57	2.06±0.12	26	0.55				
35	208	9023	5,7	1.67±0.38	0.39	2.10±0.14	26	0.64				
36	209	9033	3,7	1.47±0.31	0.45	1.77±.010	26	0.73				

Table 1: Best-fit parameters of power law and Compton model for the thirty-six selected single-day spectra

GROJ0422+32

- The high-intensity spectrum has two components: a comptonized component <300 keV plus a power-law component >300 keV
- The low-intensity spectrum has a power-law shape from ~ 30 keV to ~ 1 MeV
- The high-intensity and low-intensity spectra intercept at ~ 600 keV
- Episodic hard 0.4-1 MeV emission was observed(VP-42) with spectral index of ~ 1

Cygnus X-1

- The γ_2 (Ling et al. 1987; 1997), or "low/hard" x-ray state spectrum, has two components: a comptonized component <300 keV plus a power-law component >300 keV
- The γ_0 (Phlips et al. 1996; Ling et al. 1997; McConnell et al. 2000, 2002), or "high/soft" x-ray state spectrum has a power-law shape from ~ 30 keV to ~ 10 MeV (Phlips et al. 1996; Ling et al. 1997; McConnell et al. 2000, 2002)
- The γ_2 and γ_0 spectra intercept at ~ 1 MeV (McConnell et al. 2002)
- Episodic broad "MeV" feature with possibly a correlated narrow 511 keV annihilation feature were observed by HEAO-3 in the "superlow" state (γ_1) spectrum (Ling et al. 1987; Ling & Wheaton 1989)

Table 2: GROJ0422+32 & Cygnus X-1 Comparison